



Observation of Damage Initiation for Trans-laminar Fracture Using in situ Fast Synchrotron X-ray Radiography and ex situ X-ray Computed Tomography

Xiaodong Xu¹ · Nathanael Leung² · Urangua Jargalsaikhan² · Evi Bongaers³ · Tan Sui²

Received: 1 November 2023 / Accepted: 7 February 2024 / Published online: 21 February 2024
© The Author(s) 2024

Abstract

Trans-laminar fracture is an important topic for engineering composites. In this study, trans-laminar fracture initiation in quasi-isotropic carbon/epoxy laminates made of non-crimp fabrics was examined using in situ fast synchrotron X-ray radiography and ex situ X-ray computed tomography. The maximum split lengths were measured by in situ radiography and were compared with the predicted values in a detailed FE model using cohesive elements. Ex situ computed tomography scans were also conducted to confirm that no fibre breakage occurs before the final load drop in the experiments. In situ and ex situ observations are complementary for the understanding of damage initiation.

Keywords Fracture · Fracture Toughness · CT Analysis · Synchrotron X-ray Radiography

1 Introduction

The application of carbon fibre composites in engineering fields has grown over the last few decades, primarily due to their outstanding specific strength and stiffness [1]. Another important material property of these composite materials is their resilience, measured in terms of fracture toughness. However, the knowledge of the fracture mechanisms, especially with regard to trans-laminar fracture, still requires further investigations [2].

✉ Xiaodong Xu
xiaodong.xu@cranfield.ac.uk

✉ Tan Sui
t.sui@surrey.ac.uk

¹ Centre for Aeronautics, School of Aerospace, Transport and Manufacturing, Cranfield University, Cranfield MK43 0AL, U.K.

² School of Mechanical Engineering Sciences, University of Surrey, Guildford, Surrey GU2 7XH, U.K.

³ Neoscan BV, Wayenborgstraat 3, Mechelen 2800, Belgium

Detailed observations of trans-laminar fracture propagation are important for understanding how composite materials fail. Digital Image Correlation (DIC) is a widely used method for observing the damage progression in real-time [3, 4]. However, the method is mainly limited to the specimen surface which is more problematic given that these composites often consist of multiple plies through thickness with different orientations. In contrast, *ex situ* X-ray Computed Tomography (CT) can overcome such limitation of DIC, so has been used for examining trans-laminar fracture with different specimen sizes [5], material architectures [6] and layups [7] often with dye penetrant to enhance contrast. Furthermore, *in situ* CT analysis has been used to investigate trans-laminar fracture initiation [8] and initial propagation [9], offering continuous observations while the specimen is being loaded. *In situ* synchrotron X-ray CT has also been adopted to investigate damage evolution in composites [10], and it was concluded that complementary *ex situ* CT scans [11] can improve understanding in addition to the existing *in situ* scans [10].

Trans-laminar fracture is a complex phenomenon because there is not a clear through-thickness crack but a process zone which consists of fibre breakage, delamination and splitting. Much of the recent works done so far on trans-laminar fracture have been about some key failure mechanisms during fracture propagation [6, 7, 9, 12], and only some early studies were focused on the evolution of sub-critical damage. For example, Ciba Geigy's T300/914 C cross-ply laminates were examined with X-ray radiography [13] and transparent Hexcel's E-glass/913 cross-ply laminates were examined visually [14] to quantify 0° split lengths at the crack tip. Few quantitative studies on splitting were done using quasi-isotropic carbon/epoxy laminates. Xu et al. [15] conducted a numerical study which showed that the growth of 0° splits is driven by strain energy, but the predicted split lengths were not validated by experiments.

In the current study, an *in situ* fast synchrotron X-ray radiography enables continuous examinations of damage evolution at the crack tip of quasi-isotropic carbon/epoxy laminates. The *in situ* observation of splitting offers new insights into the initiation of trans-laminar fracture. The measured maximum split lengths follow a similar trend compared to that predicted by the detailed Finite Element (FE) method using cohesive elements. The *ex situ* X-ray computed tomography scans offer complementary results confirming no fibre breakage occurred until the end of the experiments.

2 Materials and Methods

2.1 Materials

A test panel, with a nominal laminate thickness of 2 mm, was manufactured at the Japan Aerospace Exploration Agency (JAXA) via Vacuum assisted Resin Transfer Moulding (VaRTM). The material used was bi-axial carbon Non-Crimp Fabric (NCF) made from STS-24k fibres (SAERTEX Co. KG), and DENETITE™ epoxy resin (XNR6809/XNH6809, Nagase Chemtex Co). The stacking sequence used was $[(45/-45)/(0/90)]_2s$. The specimens were then cut from the panel using 1 mm carbide end mills on an Auto Lab milling machine system (MITS Electronics, Japan).

In this work, three compact tension specimens (S1, S2, and S3) were used for the *in situ* micromechanical testing combined with a fast synchrotron X-ray radiography and another

three specimens (S4, S5, and S6) for interrupted tests followed by ex situ computed tomography (CT) scans. An engineering drawing of the specimen and an illustration of the ply orientations are shown in Fig. 1a.

2.2 Deben Testing jig Design

A test jig (Fig. 1c) was designed to perform compact tension testing on a Deben MT5000 micromechanical testing stage, for both in situ synchrotron X-ray radiography and the interrupted tests for ex situ CT scanning. The specimen was held upright to avoid the potential interference of the steel jig to the X-ray beam.

2.3 In situ Micromechanical Testing with Radiography

The in situ radiographic experiment was performed on the B16 beamline at Diamond Light Source (DLS, UK). To monitor crack growth, a PCO.edge CCD camera was set-up ~ 640 mm behind the samples, to gather radiographic data with a pixel resolution of $1.1 \mu\text{m}$ and a field of view (FOV) of 2.3×2.0 mm.

A Deben MT5000 Microtest rig (Microtest, Deben Ltd., Suffolk, UK) was used to perform an elastic compliance technique on the compact tension specimens whilst continuous radiography scans were acquired. The load-displacement graph obtained from the in situ radiography experiment performed on the three specimens can be seen in Fig. 2a. Overall, 13 cycles, 15 cycles, and 12 cycles were achieved for in Specimen 1 (S1), Specimen 2 (S2), and Specimen 3 (S3), respectively.

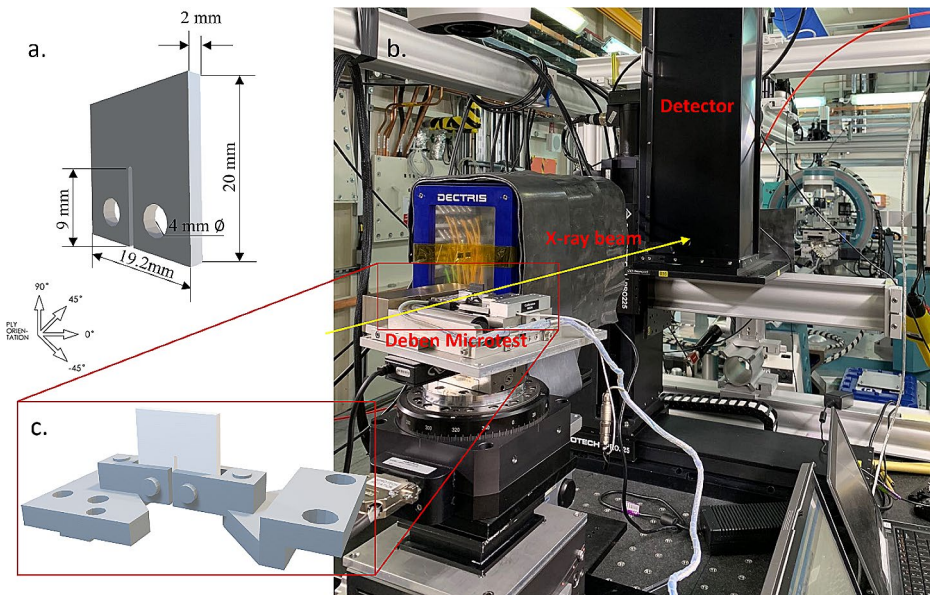


Fig. 1 (a) Engineering drawing of the carbon/epoxy composite compact tension specimen; (b) In situ synchrotron X-ray radiography set-up; (c) Customized Deben micromechanical test jig

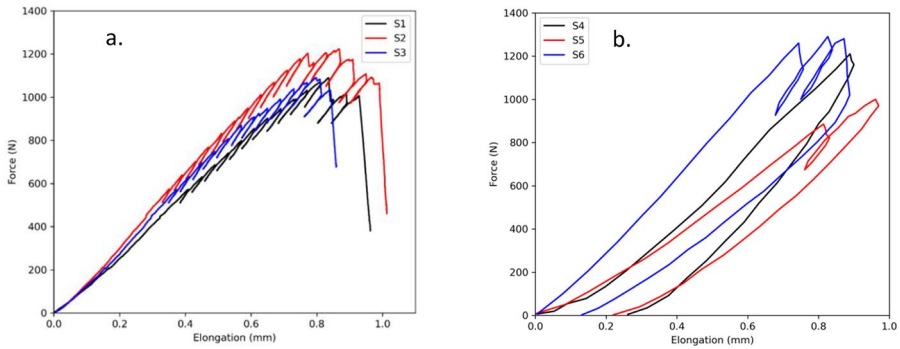


Fig. 2 Deben Force-elongation curves for (a) S1, S2 and S3 during in situ radiography experiments; (b) S4, S5 and S6 during interrupted experiments before X-ray CT

2.4 Ex situ Computed Tomography

Prior to the ex situ CT scanning, three interrupted tests were performed involving three different load-unload regimens for each specimen as shown in Fig. 2b. In the first specimen (S4), the specimen was loaded until a load drop was observed at 1200 N. In the second specimen (S5), the specimen was loaded until a load drop occurred, at which point the specimen was partially unloaded and then loaded again until a second load drop was observed at 1000 N. Finally, for the third specimen (S6), the specimen was loaded and unloaded until three load drops were observed with the last load drop at 1280 N. The measured displacements from the interrupted tests in Fig. 2b are not used for any assessments. After the three interrupted tests, S4, S5 and S6 were scanned using the NeoScan S80 CT scanner with a 5 μm pixel size.

2.5 Fracture Toughness Calculations

Referring to the ASTM E399 standard [16], the Mode I stress intensity factor (K_I) was calculated using the following equation:

$$K_I = \frac{P}{B\sqrt{W}}f\left(\frac{a}{W}\right) \tag{1}$$

where P is the paused load, B is the specimen thickness, W is the width from the specimen rear end to the centre of holes, and a is the initial crack length of the specimen. For the compact tension specimen, the geometry function $f(a/W)$ is given by:

$$f\left(\frac{a}{W}\right) = \frac{\left(2 + \frac{a}{W}\right)}{\left(1 - \frac{a}{W}\right)^{3/2}} \left[0.886 + 4.64\frac{a}{W} - 13.32\left(\frac{a}{W}\right)^2 + 14.72\left(\frac{a}{W}\right)^3 - 5.6\left(\frac{a}{W}\right)^4 \right] \tag{2}$$

The reason for using the initial machined crack length in all calculations is because no crack growth was observed except in the 0° plies of one specimen which will be discussed later.

Therefore, only the stress intensity factors before any crack growth were used. The Mode I strain energy release rate is calculated according to Eq. 3 with $E=37.9$ GPa [17], assuming plane stress:

$$G_I = \frac{K_I^2}{E} \tag{3}$$

2.6 Finite Element Analysis

Xu et al. [15] developed a detailed ply-by-ply FE model with a sharp notch in LS-Dyna using cohesive elements for intralaminar splitting and interlaminar delaminations. The traction-separation law for cohesive elements is shown in Fig. 3a. The input properties used were $G_{IC} = 0.2$ N/mm, $G_{IIc} = 1$ N/mm, $\sigma_I^{max} = 60$ MPa and $\sigma_{II}^{max} = 90$ MPa.

It was found that the 0° splits increase linearly with strain energy release rates without considering fibre failure. By revisiting the previous model [15], new results are extracted for all splits represented by the failed cohesive elements as shown in Fig. 3b. The predicted maximum split length is in the surface 45° plies. The predicted maximum split lengths at different strain energy release rates are compared against the experimental results.

3 Results and Analysis

All radiography and CT images in this work were reconstructed by Thermo Fisher Scientific’s Avizo and enhanced and analysed by Comet Technologies’ Dragonfly. All split lengths were measured using Image J.

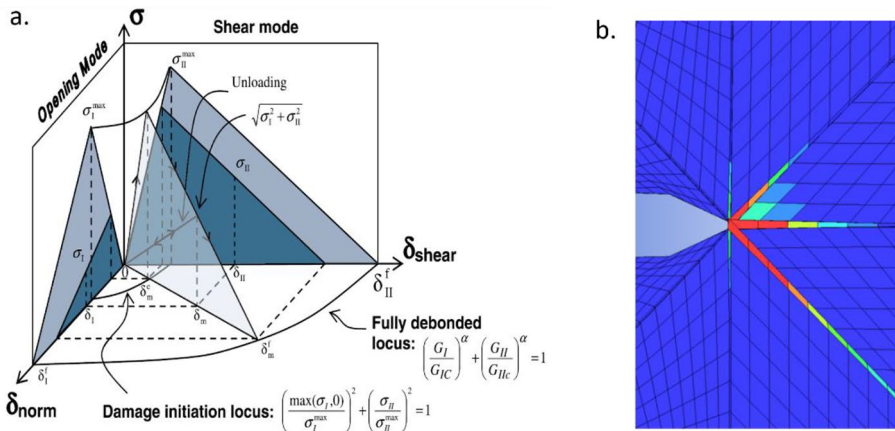


Fig. 3 A detailed FE method for predicting damage initiation using cohesive elements with (a) Traction-separation relationship [18]; (b) Failed cohesive elements in red

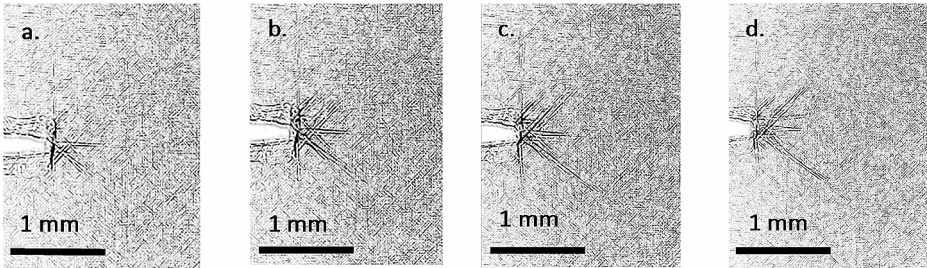


Fig. 4 Representative radiograph images taken from S3 during the in situ radiography experiment (cycle 1, 5, 9, 13) at (a) 585 N; (b) 754 N; (c) 958 N; (d) 1074 N

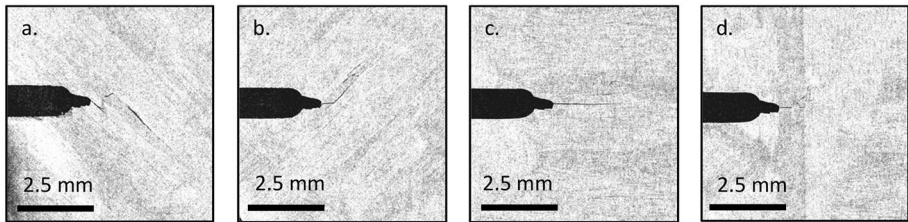


Fig. 5 CT images showing damage from S6 after the peak load at 1280 N in (a) 45° ply; (b) -45° ply; (c) 90° ply; (d) 0° ply

3.1 In situ Micromechanical Test Results

In situ radiography offered continuous examination and a good resolution. This is preferable when studying splitting also because the specimen is loaded so the cracks are open. The multiple matrix crack propagation near the crack tip was successfully visualized. Fig. 4 shows the typical radiographic images at different loads during an in situ test. These radiographic images show the overall damage zone including 0°, $\pm 45^\circ$ and 90° splits in all plies, but no obvious fibre failure by 1074 N. The maximum split length in the specimen can be measured which is in the 45° plies.

3.2 Ex situ CT Scanning Results

While in situ radiography provided continuous examination of overall damage evolution, ex situ CT scanning was also done to show the cracks at different depths (plies) through the specimen thickness. This is difficult to observe in in situ radiography images because the damage in all plies is overlapped. Typical CT scan images in Fig. 5 show the damage states in different plies of Specimen S6 interrupted after 1280 N. It shows that fibers broke in the $\pm 45^\circ$ and 0° plies at the final load drop, but further examination prove that fibers did not break at the first load drop in S4 and the second load drop in S5 as shown in Fig. 6. Splitting is visible in Fig. 5 except for the 0° ply in Fig. 5d. This is because the splitting was closed when the specimen was scanned after being unloaded.

Compared to the CT scan images in Fig. 5 from the interrupted tests, the in situ X-ray radiographic images in Fig. 4 provide sufficient phase contrast and resolution for continu-

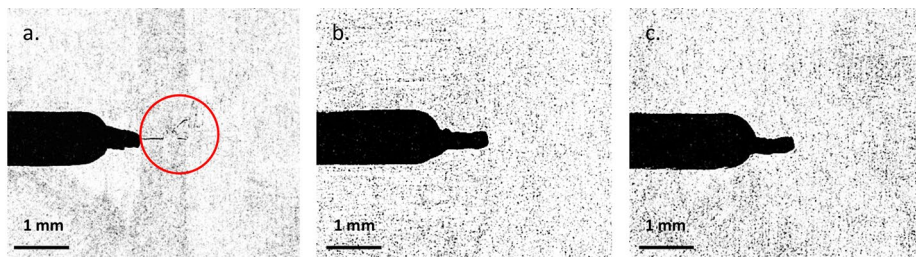


Fig. 6 CT images showing fibre breakage circled in the 0° plies in (a) S6, and lack of fibre breakage in (b) S5 and (c) S4 after peak loads

ous measurements of splitting during trans-laminar fracture initiation before fibre fracture occurs. In Fig. 2a, the load-displacement curves from the in situ radiography experiments show consistent trends for all three specimens. Fig. 6 shows the presence of fibre fracture after the last load drop in Specimen S6 (1280 N), but no fibre breakage was observed in S4 (1200 N) and S5 (1000 N). Therefore, it is not expected to have fibre failure in Specimens S1 to S3 under 1200 N.

3.3 Results and Discussion

The strain energy release rate of each specimen is determined by the initial crack length according to Eq. 1 to 3. Therefore, the maximum split length of three specimens (S4, S5 and S6) in relation to strain energy release rate is established as shown in Fig. 7. Among all the splits, the 45° splits are the longest and the most prominent in the images, so they are measured for comparison. The results show that the maximum split lengths grow approximately linearly with strain energy release rates.

Recently, trans-laminar fracture initiation in quasi-isotropic carbon/epoxy laminates was studied [8]. The fracture process zone development was monitored using in situ X-ray CT scanning. The scans were conducted while the specimens were still loaded. The damage sequence throughout the in situ tests was presented. Splitting was found early on during the tests, which agrees with the current findings. No detailed numerical study was included for trans-laminar fracture initiation in the work [8].

Another recent detailed numerical study of trans-laminar fracture [19] was mainly focused on the prediction of R-curve behaviour during fracture propagation, which followed an earlier numerical work on fracture process zone development [15]. In Fig. 7, the currently measured slope is similar to that for the maximum splits predicted using the detailed model [15]. This suggests that the maximum splitting is driven by the same strain energy. The independent in situ radiography results in this work can confirm the findings of the detailed FE results. It is noted that the current slope for the maximum splitting in Fig. 7 is different from the previously reported slope for the 0° splitting, with the former being steeper.

This work demonstrates that in situ radiography and ex situ X-ray CT scanning are complementary for the study of trans-laminar fracture initiation. The former offers continuous examination of overall damage while the latter provides a ply-by-ply damage map from interrupted tests. Combining both techniques, the growth of split lengths can be identified and quantified before fibres are broken. This potentially leads significant benefit e.g. for

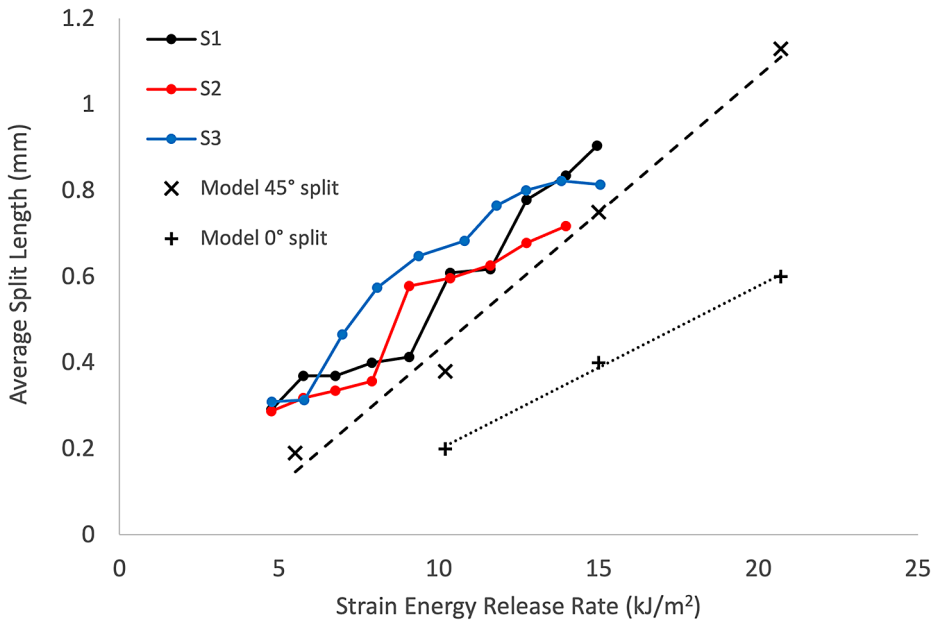


Fig. 7 Maximum split length – strain energy release rate graph from in situ radiography experiments and FE model

assessing fatigue damage and residual strength of aircraft composites which are subject to a load much lower than the ultimate failure load.

4 Conclusions

Damage initiation in quasi-isotropic carbon/epoxy laminates made of non-crimp fabrics was examined experimentally using in situ fast synchrotron X-ray radiography and ex situ X-ray computed tomography. In situ radiography shows that maximum split length in the 45° plies of the quasi-isotropic laminates was driven by strain energy. It also agrees with the predicted trend of maximum splitting in a previous detailed FE model using cohesive elements without considering fibre failure.

Ex situ computed tomography confirms that no fibre breakage occurred before the load drops under 1200 N. As a result, the initial machined notch did not extend before this point i.e. trans-laminar fracture did not propagate. The experimental results are therefore comparable with the FE results which also do not consider fibre failure. In situ and ex situ observations are complementary for understanding trans-laminar fracture initiation.

Acknowledgements Tan Sui (TS) would like to thank Dr Igor Dolbnya, from the B16 beamline at Diamond Light Source (DLS), for his support and assistance with the synchrotron X-ray experimental setup and data acquisition. DLS is also acknowledged for providing access to the B16 beamline under the allocation MM23174. TS thanks Dr Jingyi Mo for her support and assistant with initial data analysis for ex situ experiments. TS also acknowledges support from the Engineering and Physical Sciences Research Council (EP/S022813/1). Xiaodong Xu would like to thank Dr Shin-ichi Takeda, from Japan Aerospace Exploration Agency (JAXA), for allowing him to use JAXA material for this research.

Author Contributions Xiaodong Xu: Conceptualization, Methodology, Investigation, Software, Writing – original draft. Nathanael Leung: Methodology, Investigation, Formal analysis, Writing – original draft. Urangua Jargalsaikhan: Methodology, Investigation, Writing – original draft. Evi Bongaers: Methodology, Investigation, Writing – Reviewing & Editing. Tan Sui: Conceptualization, Methodology, Investigation, Resources, Writing – Reviewing & Editing, Supervision, Project administration, Funding acquisition.

Funding B16 beamline at Diamond Light Source under the allocation MM23174 (Tan Sui). Engineering and Physical Sciences Research Council EP/S022813/1 (Tan Sui).

Data Availability The raw/processed data required to reproduce these findings will be made available on request.

Declarations

Ethical Approval Not applicable.

Competing Interests The authors declare no competing interests.

Open Access This article is licensed under a Creative Commons Attribution 4.0 International License, which permits use, sharing, adaptation, distribution and reproduction in any medium or format, as long as you give appropriate credit to the original author(s) and the source, provide a link to the Creative Commons licence, and indicate if changes were made. The images or other third party material in this article are included in the article's Creative Commons licence, unless indicated otherwise in a credit line to the material. If material is not included in the article's Creative Commons licence and your intended use is not permitted by statutory regulation or exceeds the permitted use, you will need to obtain permission directly from the copyright holder. To view a copy of this licence, visit <http://creativecommons.org/licenses/by/4.0/>.

References

1. Ishikawa, T., Amaoka, K., Masubuchi, Y., Yamamoto, T., Yamanaka, A., Arai, M., Takahashi, J.: Overview of automotive structural composites technology developments in Japan. *Compos. Sci. Technol.* **155**, 221–246 (2018). <https://doi.org/10.1016/j.compscitech.2017.09.015>
2. Laffan, M.J., Pinho, S.T., Robinson, P., McMillan, A.J.: Translaminar fracture toughness testing of composites: A review. *Polym. Test.* **31**, 481–489 (2012). <https://doi.org/10.1016/j.polymertesting.2012.01.002>
3. Catalanotti, G., Camanho, P.P., Xavier, J., Dávila, C.G., Marques, A.T.: Measurement of resistance curves in the longitudinal failure of composites using digital image correlation. *Compos. Sci. Technol.* **70**, 1986–1993 (2010). <https://doi.org/10.1016/j.compscitech.2010.07.022>
4. Zobeiry, N., Vaziri, R., Poursartip, A.: Characterization of strain-softening behavior and failure mechanisms of composites under tension and compression. *Compos. Part. Appl. Sci. Manuf.* **68**, 29–41 (2015). <https://doi.org/10.1016/j.compositesa.2014.09.009>
5. Xu, X., Wisnom, M.R., Mahadik, Y., Hallett, S.R.: Scaling of fracture response in over-height compact tension tests. *Compos. Part. Appl. Sci. Manuf.* **69** (2015). <https://doi.org/10.1016/j.compositesa.2014.11.002>
6. Rev, T., Nachman, T., Kap, I., Shor, O., Shemesh, N., Mollenhauer, D., Rittel, D.: Architecture effects for mode I trans-laminar fracture in over-height compact tension tests: Damage propagation and fracture response. *Compos. Part. Appl. Sci. Manuf.* **159**, 106987 (2022). <https://doi.org/10.1016/j.compositesa.2022.106987>
7. Xu, X., Sun, X., Wisnom, M.R.: Initial R-curves for trans-laminar fracture of quasi-isotropic carbon/epoxy laminates from specimens with increasing size. *Compos. Sci. Technol.* **216**, 109077 (2021). <https://doi.org/10.1016/j.compscitech.2021.109077>
8. Xu, X., Takeda, S., Wisnom, M.R.: Investigation of fracture process zone development in quasi-isotropic carbon/epoxy laminates using in situ and ex situ X-ray computed Tomography. *Compos. Part. Appl. Sci. Manuf.* **166**, 107395 (2023). <https://doi.org/10.1016/j.compositesa.2022.107395>
9. Sun, X., Takeda, S., Wisnom, M.R., Xu, X.: In situ characterization of trans-laminar fracture toughness using X-ray computed Tomography. *Compos. Commun.* **21**, 100408 (2020). <https://doi.org/10.1016/j.coco.2020.100408>

10. Jo, E., Lee, S., Hong, C., Ji, W.: In situ observation of interactive failure modes in a single-edge notched symmetric cross-ply laminate using synchrotron X-ray tomography. *Compos. Part. Appl. Sci. Manuf.* **128**, 105661 (2020). <https://doi.org/10.1016/j.compositesa.2019.105661>
11. Hong, C., Ji, W.: Complementary ex situ investigations of various fracture modes in a single-edge-notched symmetric cross-ply laminate subjected to tensile loading. *Compos. Commun.* **17**, 28–31 (2020). <https://doi.org/10.1016/j.coco.2019.11.004>
12. Gong, B., Ge, Y., Wang, H., Peng, H.-X., Wisnom, M.R., Xu, X.: Hygrothermal effects on translaminar fracture toughness of quasi-isotropic laminates with different stacking sequences. *Compos. Commun.* **45**, 101791 (2024). <https://doi.org/10.1016/j.coco.2023.101791>
13. Kortschot, M.T., Beaumont, P.W.R.: Damage mechanics of composite materials: I- measurements of damage and strength. *Compos. Sci. Technol.* **39**, 289–301 (1990). [https://doi.org/10.1016/0266-3538\(90\)90077-1](https://doi.org/10.1016/0266-3538(90)90077-1)
14. Hallett, S.R., Wisnom, M.R.: Experimental investigation of progressive damage and the Effect of Layup in Notched Tensile tests. *J. Compos. Mater.* **40**, 119–141 (2006). <https://doi.org/10.1177/0021998305053504>
15. Xu, X., Wisnom, M.R., Li, X., Hallett, S.R.: A numerical investigation into size effects in centre-notched quasi-isotropic carbon/epoxy laminates. *Compos. Sci. Technol.* **111** (2015). <https://doi.org/10.1016/j.compscitech.2015.03.001>
16. ASTM E399-90: Standard test method for plane-strain fracture toughness of metallic materials. In: *ASTM Book of Standards*. ASTM INTERNATIONAL, West Conshohocken (1997)
17. Xu, X., Takeda, S., Aoki, Y., Hallett, S.R., Wisnom, M.R.: Predicting notched tensile strength of full-scale composite structures from small coupons using fracture mechanics. *Compos. Struct.* **180**, 386–394 (2017). <https://doi.org/10.1016/j.compstruct.2017.08.026>
18. Jiang, W.-G., Hallett, S.R., Green, B.G., Wisnom, M.R.: A concise interface constitutive law for analysis of delamination and splitting in composite materials and its application to scaled notched tensile specimens. *Int. J. Numer. Methods Eng.* **69**, 1982–1995 (2007). <https://doi.org/10.1002/nme.1842>
19. Xu, X., Wisnom, M.R., Hallett, S.R.: Deducing the R-curve for trans-laminar fracture from a virtual over-height Compact Tension (OCT) test. *Compos. Part. Appl. Sci. Manuf.* **118**, 162–170 (2019). <https://doi.org/10.1016/j.compositesa.2018.12.027>

Publisher's Note Springer Nature remains neutral with regard to jurisdictional claims in published maps and institutional affiliations.